Duration-limited growth method for wind sea and swell separation of directional wave spectrum

Lee, Yu Chen; Doong, Dong Jiing

DOI
10.1016/j.oceaneng.2025.121182

Publication date
2025

Document Version
Final published version

Published in
Ocean Engineering

Citation (APA)
Lee, Y. C., & Doong, D. J. (2025). Duration-limited growth method for wind sea and swell separation of directional wave spectrum. *Ocean Engineering*, *329*, Article 121182. https://doi.org/10.1016/j.oceaneng.2025.121182

Ocean Engineering 329 (2025) 121182

Contents lists available at ScienceDirect

Ocean Engineering

journal homepage: www.elsevier.com/locate/oceaneng

Research paper

Duration-limited growth method for wind sea and swell separation of directional wave spectrum

Yu-Chen Lee [a,b], Dong-Jiing Doong [a,c,*]

[a] Coastal Ocean Monitoring Center, National Cheng Kung University, Tainan, Taiwan
[b] Delft Center for Systems and Control, Faculty of Mechanical Engineering, Delft University of Technology, Delft, the Netherlands
[c] Department of Hydraulic and Ocean Engineering, National Cheng Kung University, Tainan, Taiwan

ARTICLE INFO

Keywords:
Wind sea and swell separation
Directional wave spectrum
Duration-limited wave growth
Wave refraction
Wave forecasting and analysis

ABSTRACT

The separation of wind sea and swell is crucial for advancing wave dynamics research, improving wave forecasting, and optimizing the design of coastal and offshore structures. In this study, we highlight the limitations of the widely used wave age method for separating two-dimensional wind sea and swell. Specifically, under strong wind conditions, waves require extended durations to reach full development—an aspect not accounted for by the wave age method, which assumes fully developed seas and thus tends to overestimate wind sea. Furthermore, changes in wind direction and wave refraction in shallow waters can lead to misclassification. To overcome these issues, we propose a novel algorithm for directional spectral separation, grounded in wind wave growth theory and incorporating wave refraction effects. The proposed method improves separation accuracy and delivers more consistent results across a range of wave conditions.

1. Introduction

The sea state is generally composed of two main types of surface waves, wind sea and swell. Wind sea refers to waves generated by local winds, characterized by short wavelengths, greater steepness, and higher frequencies. These waves result from the direct transfer of energy from the wind to the water surface and are often chaotic and irregular. In contrast, swells are longer-period waves that propagate over extensive distances from their region of generation, typically originating from distant storms or wind systems. These waves have longer wavelengths and longer crests, and their energy can persist over a long distance as they propagate across the ocean with minimal dissipation during evolution. The arrival time of the swell is considered a practical parameter for coastal hazard forecasting (Delpey et al., 2010; Ardhuin et al., 2016; Jiang et al., 2016). The interaction between wind sea and swell determines the wave dynamics of the overall sea state. The coexistence of wind sea and swell often manifests as two or more peaks in the spectrum, reflecting the presence of different atmospheric sources. The probability of double-peaked spectra occurrences was shown to be 22 % on average (Guedes Soares, 1991) and ranged from 23 % to 26 % (Guedes Soares and Nolasco, 1992) in the North Atlantic Ocean. However, the number of peaks in the spectra varies significantly across different datasets, influenced by the ocean's geographical and atmospheric conditions. In Taiwan waters, it is observed that approximately 8.8 % of the measured buoy dataset was double-peaked based on our investigation. These multi-modal sea states have a significant impact on the design and operability of fixed and floating offshore structures (Ewans et al., 2006; Muraleedharan et al., 2010). Notably, numerical wave models, such as WaveWatch III, employ the concept of wave age to parameterize the wind input source term (Tolman, 2009). From an observational perspective, a critical challenge lies in accurately identifying and characterizing swells, as long-period swells propagating from distant storm systems often pose significant hazards to offshore and coastal areas (Yuk et al., 2016; Zhang and Li, 2017; Wandres et al., 2020). Additional tests on the forces in mooring lines and fenders at oil and gas terminals were conducted, and the simulations concluded that swell waves are the dominant factor in mooring loads (van der Molen et al., 2003). Polidoro et al. (2018) demonstrate that the existence of long-period energy was the leading cause of the beach profile response under bimodal wave conditions, and the numerical models were found to notably underestimate the beach crest erosion. These impacts highlight the importance of methods for separating wind sea and swell energy, which has become a major area of interest for experts and researchers across various application scenarios.

* Corresponding author. Coastal Ocean Monitoring Center, National Cheng Kung University, Tainan, Taiwan.
E-mail address: doong@mail.ncku.edu.tw (D.-J. Doong).

https://doi.org/10.1016/j.oceaneng.2025.121182
Received 29 December 2024; Received in revised form 31 March 2025; Accepted 6 April 2025
Available online 14 April 2025

The wind sea and swell separation method is mainly divided into two types based on the wave spectrum. For one-dimensional wave spectra, the separation of wind sea and swell depends on the determination of a separation frequency f_s (Earle, 1984; Wang and Gilhousen, 1998; Wang and Hwang, 2001; Portilla et al., 2009; Hwang et al., 2012). Wave energy at frequencies higher than f_s is considered generated by local winds; wave energy at frequencies lower than f_s is considered generated by swell. Additionally, the curve of fully developed seas based on wave height and wind speed can also be used to identify wind sea and swell, as wind sea cannot exceed fully developed sea states (Chen et al., 2002; Jiang and Chen, 2013; Jiang and Yang, 2022). Earle (1984) proposed that the separation frequency has a linear relation with the peak frequency of the Pierson–Moskowitz (PM) spectrum, which can be determined for a given local wind speed. Wang and Hwang (2001) proposed a wave steepness method based on the theory that the characteristics of the steepness function are more related to the high-frequency wind sea components. This method relies on 1D wave spectra instead of wind information, which can be implemented for operational applications. Portilla et al. (2009) found that the wave steepness method proposed by Wang and Hwang (2001) may systematically overestimate swell. They compared the wave spectrum energy to a fully developed spectrum and proposed a PM peak method to identify wind sea and swell. Hwang et al. (2012) proposed a revised spectrum integration method improving the shortcomings of the wave steepness method, which performs poorly in high winds and when wave ages differ significantly from 1. A recent study by Zheng et al. (2024) has further explored finite water depth conditions based on the TMA spectrum, thereby enhancing the PM peak method of Portilla et al. (2009). Meng et al. (2023) further applied data-driven methods to develop a new 1D wind sea and swell separation method.

The 2D wind sea and swell separation methods consider wind and wave directions to solve the overlap of wave systems in the frequency domain. This method consists of two steps: spectral partitioning and partition identification. The partitioning scheme based on the inverse watershed algorithm separates the spectrum into several partitions corresponding to distinct meteorological events (Gerling, 1992; Hasselmann et al., 1996; Portilla et al., 2009). The identification scheme categorizes each partition as wind sea or swell based on wave age criteria, also known as the wave age method (Komen et al., 1984; Hanson and Phillips,2001; Portilla et al., 2009). The 2D method demonstrates greater reliability compared to the 1D process, as it considers additional factors such as directional distribution, wind speed, and wind and wave direction in the separation of wind sea from swell (Portilla et al., 2009; Chen et al., 2015).

When applying the 2D wind sea and swell separation method, we found that it produced unexpected results, which will be further discussed in this study. We selected several cases from field measurement data around Taiwan waters that include the aforementioned issues. We will discuss the newly proposed wind sea and swell separation method as a solution to these challenges.

Our paper is structured as follows: Section 2 provides a brief overview of the wind sea and swell separation methods discussed in the literature. Section 3 introduces the data collection and selection process used in this study. Section 4 highlights the limitations of current approaches identified in the selected data. To address these issues, we propose a new method based on wave growth theory, detailed in Section 5. We also apply this method to the data to demonstrate its improvements in Section 6. Finally, Section 7 presents our conclusions.

2. Methods

2.1. One-dimensional wind sea and swell separation methods

The PM peak method (Portilla et al., 2009) and spectrum integration method (Hwang et al., 2012) were commonly used to identify wind sea and swell components in the 1D spectrum. These methods have an apparent advantage that can be easily implemented by the 1D wave spectrum without the additional wind information. The 1D methods generally determine a separation frequency f_s to separate the wave energy into wind sea at higher frequencies and swell at lower frequencies. This study draws comparisons among the PM peak method, the spectrum integration method, and the wave age method, presenting the following results.

The PM peak method utilizes the peak enhancement factor γ of the JONSWAP spectrum to identify wind sea and swell, where γ represents the peak energy enhancement compared to a fully developed spectrum. This parameter represents the active wave growth, meaning that the peak amplitude of the developing wind sea is greater than the swell with the same peak frequency. The peak enhancement factor γ can be expressed by the ratio of the peak of the measured spectrum and the PM spectrum:

$$\gamma = \frac{S\left(f_p\right)}{S_{PM}\left(f_p\right)} \tag{1}$$

where $S\left(f_p\right)$ is the peak value of the 1D wave spectrum and $S_{PM}\left(f_p\right)$ is the same peak frequency corresponding to the PM spectrum. This factor is used to identify wind sea and swell in the PM peak method. Every peak of the wave partition needs to be classified based on this criterion: If $\gamma > 1$, the form of the field spectrum is sharper than the PM spectrum, which is identified as wind sea; otherwise, it will be considered as swell.

Another method by Hwang et al. (2012) called spectrum integration method, which is revised from the wave steepness method (Wang and Hwang, 2001). Portilla et al. (2009) found that the wave-steepness method overestimated swell during wind sea dominant periods because the separation frequency is higher than the wind sea peak frequency. Hwang et al. (2012) pointed out two major shortcomings of the wave-steepness method which are:(a) the method is only designed on the inverse wave age $U_{10}/\ C_{pw} = 1$, where the subscript *pw* denotes the peak of the wind sea; and (b) for an analytical power-law spectrum with a -4-slope high-frequency tail, the peak of the wave-steepness function, $\xi(f)$, may not downshift monotonically as wind speed increases. They developed the spectrum integration method to solve shortcomings of the previous wave steepness method. In the spectrum integration method, the energy spectrum is changed to $S(f)/f^b$ and setting $b \geq 1$. This spectrum integration holds an advantage in smoothing out the spikiness of the wave spectrum. The revised function $I_b(f)$ can be expressed as:

$$I_b(f) = \frac{\int_{\mathrm{f}}^{f_u} f'^2 \left[S(f')\Big/ f'^b\right] df'}{\sqrt{\int_{\mathrm{f}}^{f_u} \left[S(f')\Big/ f'^b\right] df'}} \tag{2}$$

This algorithm is based on searching for the maximum of the spectrum integration function, and the corresponding peak frequency is designated as f_{mb}. Following an analysis with simulated wave spectra, $b = 1$ is recommended. With $f_{s1} = 0.75 f_{pw}$, regression analysis applied to the field data produced the polynomial function for wind sea and swell separation frequency:

$$f_{s1} = 24.2084 f_{m1}^3 - 9.2021 f_{m1}^2 + 1.8906 f_{m1} - 0.04286 \tag{3}$$

2.2. Two dimensional wind sea and swell separation methods

The wave age method for separating wind sea and swell components in the directional spectrum is widely employed globally. This method can be classified into two parts: spectral partitioning and partition identification. The concept of spectral partitioning was initially presented by Gerling (1992). In the directional wave spectrum, the energy value determines the local energy peak based on the paths of steepest ascent. The members that lie on the collection of paths leading to the same local peak are grouped to form a spectral partition. Finally, the

directional wave spectrum was divided into distinct individual wave systems. Many partitioning schemes (Hasselmann et al., 1996; Voorrips et al., 1997; Hanson and Phillips,2001) have different settings for the combining process and a low energy threshold. However, Portilla et al. (2009) proposed an image-processing tool based on a 2D low-pass filtering step aiming to reduce noise. This scheme enhances the consistency of wave system detection, ensuring that results are not significantly affected by parameter value settings. A 2D discrete convolution operation is used to average all neighbors of a central bin and remove the spurious spectrum peaks in the directional wave spectrum, which is expressed as:

$$\widehat{S}(i,j) = k(m,n) \otimes S(i,j) = \sum_{m=-1}^{1} \sum_{n=-1}^{1} \kappa(m,n) S(i-m, j-n) \tag{4}$$

where $S(i,j)$ is the raw spectrum and $\widehat{S}(i,j)$ is the spectrum after convolution with dimensions $i \times j$. The operator $\otimes$ indicates a convolution. The convolution kernel κ is chosen as a constant $3\times$ 3 matrix with coefficients summing to unity $\left[\kappa(m,n) = \frac{1}{9}, \forall\, m, n\right]$. The convolution process is repeated until the number of partitions equal or lower between 4 and 6, so that the spectral image would not be excessively blurred and indiscernible. After partitioning, partitions with low energy relative to the total energy will be regarded as noise. These low-energy partitions are then merged with their closest adjacent partition. The settings for thresholding and combining are suggested in Portilla et al. (2009).

The identification of wind sea and swell is the utilization of wave age criterion and direction factor. This identification formulation originated from Komen et al. (1984), which depicted the evolution of a fully developed wind sea spectrum. The wave age criterion used to identify wind seas (Donelan et al., 1985; Hasselmann et al., 1996; Voorrips et al., 1997; Hanson and Phillips, 2001; Drennan et al., 2003; Portilla et al., 2009) can be shown as:

$$f_s \geq \frac{g}{2\pi}[\beta U cos(\theta - \psi)]^{-1}, |\theta - \psi| < \frac{\pi}{2} \tag{5}$$

where f_s is the separation frequency, U is the wind velocity, θ is the wave direction, ψ is the wind direction, g is the gravity acceleration, and β is a calibration factor. This criterion is derived from the deep-water dispersion relationship and is applicable only for identifying wind sea and swell under deep-water conditions. For finite water depths, the finite-depth dispersion relationship should be considered (Zheng et al., 2024). This study focuses on the discussion of wind sea growth, and further investigation into finite-depth effects is required to determine its applicability to shallow water cases.

The wave age criterion defines a parabolic region over the directional spectrum. Any peaks of partitions that belong within the parabolic region are identified as wind seas. On the contrary, the peaks of partitions that lie outside the parabolic region are considered swell. The identification results can vary significantly depending on the magnitude of the calibration factor β (Portilla et al., 2009; Chen et al., 2015). This calibration factor β ensures that all wind sea peaks correspond to the separation criterion. Old wind seas refer to wind seas that have persisted for a longer duration, allowing them to become more developed and mature. These waves generally travel faster than young wind seas. Hasselmann et al. (1996) give the range $1.3 < \beta \leq 2.0$ for the case of old wind seas. The analysis of wind sea and swell in different wave models also employs different threshold values, such as 1.3 in WAM (Voorrips et al., 1997; Bidlot, 2001) and 1.7 in WAVEWATCH III (Tracy et al., 2007). In this study, we select $\beta = 1.5$ of Hanson and Phillips (2001) for the wave age method to separate wind sea and swell.

3. Data collection and selection

The wave spectra utilized in this research are computed from time-series data collected by buoys deployed in Taiwan waters. These buoys are operated and deployed by the Coastal Ocean Monitoring Center (COMC) of the National Cheng Kung University, Tainan, Taiwan. The buoys are discus-type with a diameter of 2.5 m. Each buoy is equipped with an accelerometer with a sampling frequency of 2 Hz for 10 min every hour. The wave parameters, such as significant wave height, wave period, and wave direction, can be calculated using the accelerations, inclinations, and azimuth from the accelerometer-tilt-compass (ATC) sensor on a moored buoy. The wind anemometer is installed at the top of the buoy at approximately 3 m above mean sea level. The wind speed at the standard elevation of 10 m is obtained from the measured wind speed at 3 m height by means of the power-law wind profile (Hsu et al., 1994). The meteorological and oceanography data are checked by a data quality algorithm to assure the quality of measurements (Doong et al., 2007). The one-dimensional wave spectrum can be calculated through the Fourier transform of the heave acceleration time series, while the directional spectrum is derived from the accelerations of heave, sway, surge, roll, pitch, and yaw. The calculation of the wave spectrum by the ATC sensor was based on Lin et al. (2017). The data used in this study were collected by four stations including Longdong, Hsinchu, Xiaoliuqiu, and Taitung Open Ocean. The locations of these stations deployed in Taiwanese waters are shown in Fig. 1. Each buoy has a relatively long operational lifespan, collecting data for over ten years. The water depth range of these buoys is from 27 m to 5500 m, covering intermediate to deep water depths. Detailed information about four buoys is provided in Table 1.

We manually selected 9 wave spectra to test wind sea and swell separation methods. The main criterion for selecting them is that they may cause some errors in identification when applying the wave age method. These limitations will be described in more detail in the next section. Meanwhile, we specifically examined atmospheric conditions that could cause bimodal spectra. We found no other wind systems present that could generate additional peaks attributable to multi-peaked spectra. All the selected spectra exhibit significant double peaks, representing wind sea and swell, as shown in Fig. 2. The significant peaks in these spectra have passed the criteria for identifying spurious peaks, as defined by Portilla et al. (2009). The criteria for detecting spurious peaks are as follows: (1) the peak frequency is above 0.35 Hz, (2) the peak contains less than 5 % of the total energy, (3) the partition has fewer than 2 spectral bins, and (4) the partition has a lower peak energy than the two neighboring partitions. After applying this procedure, the significant spectral peaks are preserved, and the remaining peaks are more consistent.

In Table 2, we present the wave and wind conditions, including significant wave height H_s, mean period T_m, peak period T_p, mean wave direction Θ, wind gust U_{gust}, mean wind speed U_{mean} and wind direction ψ for 9 selected wave spectra. The wave parameters are calculated from the n-th spectral moment m_n, where $H_s = 4\sqrt{m_0}$, $T_m = \sqrt{m_0/m_2}$. Mean wind speed is typically calculated over a 10-min period, while wind gust is defined as the highest 3-s average within that same period. The statistical characteristics of these spectra include significant wave heights ranging from 1.06 m to 2.63 m, peak periods between 4.3 s and 15 s, and mean wind speeds between 9.6 m/s and 21.6 m/s. The peak period is primarily determined by the dominance of wind sea or swell. If the wind sea is dominant, it exhibits a shorter peak period, whereas a swell-dominated sea exhibits a longer peak period. The weather conditions possibly responsible for generating swell components are also shown in Table 2. The occurrence of two-peaked or multi-peaked wave spectra in Taiwan is primarily attributed to the unique atmospheric conditions, notably monsoons and typhoons. The general wave conditions in Taiwan are predominantly influenced by the monsoon, which brings southwesterly winds during the summer and northeasterly winds during

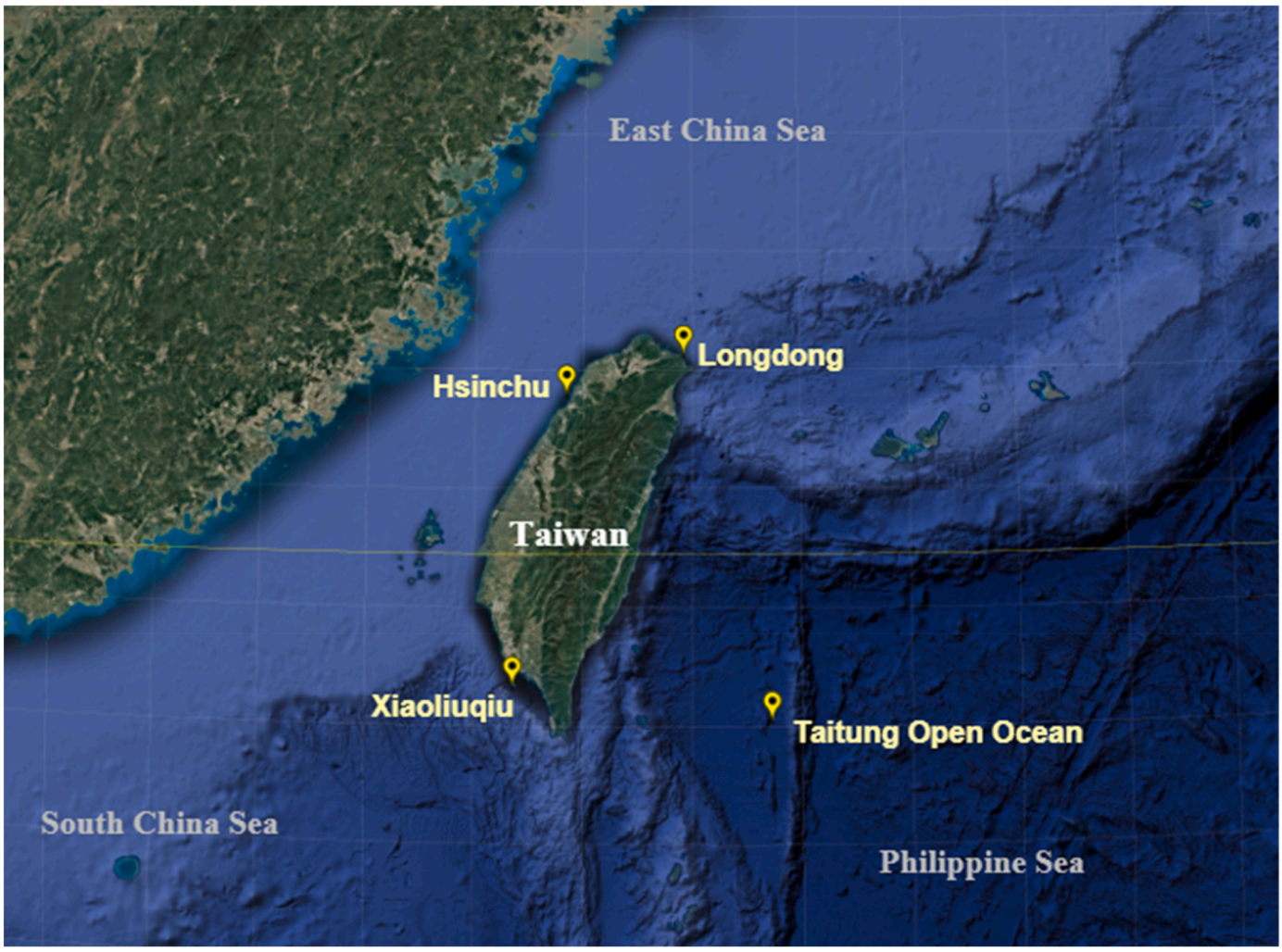

Fig. 1. Wave measurement stations in Taiwanese waters.

Table 1
In-Situ measurements information of data buoy.

Station	Duration	Coordinate	Water depth	Distance to shore	Location
Longdong	1999~2024	121°55′22″ E; 25°05′51″ N	30m	1 km	Pacific Ocean
Hsinchu	1998~2024	120°50′41″ E; 24°45′39″ N	27m	6 km	Taiwan Strait
Xiaoliuqiu	2004~2024	120°21′42″E; 22°18′46″ N	82m	4 km	Taiwan Strait
Taitung Open Ocean	2006~2024	122°43′15″ E; 22°01′26″ N	5500m	210 km	Pacific Ocean

winter. This seasonal variation has a significant impact on the development and characteristics of wind seas and swells in the China Sea (Qian et al., 2020; Hisaki, 2023). The mean peak period of swells in the waters surrounding Taiwan ranges from 9 s to 15 s based on the WAVEWATCH III model (Tao et al., 2017). Additionally, typhoons, which typically occur from July to October, generate extremely high waves and can cause significant damage. It is common for local wind seas to interact with far-field swells generated by monsoons or typhoons, resulting in a combination of wind sea and swell in the local sea states of Taiwan waters.

4. Challenges and limitations of 2D separation method

In this section, we apply the wind sea and swell separation method to our wave spectral data and find some limitations based on our results. We first present an example analyzed using the 1D PM peak method (Portilla et al., 2009), the 1D spectrum integration method (Hwang et al., 2012), and the 2D wave age method (Hanson and Phillips, 2001), as shown in the spectrum in Fig. 3. The 2D spectral partitioning method proposed by Portilla et al. (2009) was applied to the directional spectrum, followed by the application of the wave age method (Hanson and Phillips, 2001) to distinguish between wind sea and swell. The data is record #4, measured by the Hsinchu buoy at 03:00 on March 14, 2013, with a significant wave height of 2.51 m and a peak period of 10.4 s. The mean wind speed is 20.2 m/s, which corresponds to a strong wind condition (Beaufort scale 8) with a wind direction of 49° from the northeast. Fig. 3(a) shows the 1D spectrum with a double peak, where the peak with the lower frequency at 0.09 Hz was swell generated by a cold front from the East China Sea, and the peak with the higher frequency at 0.14 Hz was the wind sea generated by local winds. The separation frequencies determined by the PM peak method (Portilla et al., 2009) and the spectral integral method (Hwang et al., 2012) correspond to 0.12 Hz and 0.1 Hz, respectively. It can be observed that both separation frequencies are located between two peaks, correctly separating wind sea and swell. However, as shown in Fig. 3(b), the 2D wave age criterion (Hanson and Phillips, 2001) includes both wind sea and swell peaks in the wave age parabola. This indicates that both peaks

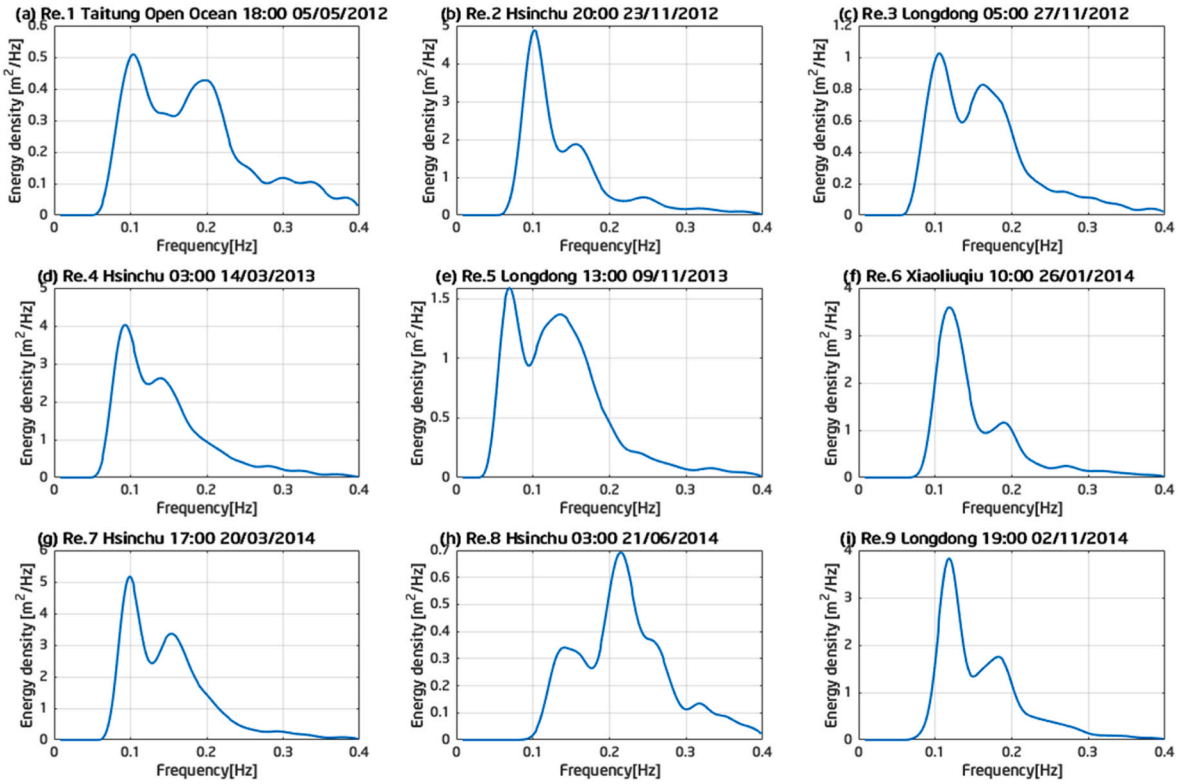

Fig. 2. One-dimensional wave spectra selected at four stations.

Table 2
Wave and wind conditions of 9 spectra used for validation.

No	Time	Buoy	H_s(m)	T_m(s)	T_p (s)	Θ(°)	U_{gust}(m/s)	U_{mean}(m/s)	ψ (°)	Weather condition
#1	2012/05/05 18:00	Taitung Open Ocean	1.06	4.8	9.8	33	11.8	9.6	335	Winter monsoon
#2	2012/11/23 20:00	Hsinchu	2.28	6.2	9.4	22	20.4	16.7	52	Winter monsoon
#3	2012/11/27 05:00	Longdong	1.34	5.5	8.6	45	13.5	9.8	357	Winter monsoon
#4	2013/03/14 03:00	Hsinchu	2.51	6.4	10.4	22	24.8	20.2	49	Winter monsoon
#5	2013/11/09 13:00	Longdong	1.71	6.5	15.0	112	15.4	12.1	167	Typhoon (Haiyan)
#6	2014/01/26 10:00	Hsinchu	1.98	5.9	8.6	11	20.2	16.6	44	Winter monsoon
#7	2014/03/20 17:00	Hsinchu	2.63	6.1	9.8	11	28.1	21.6	52	Winter monsoon
#8	2014/06/21 03:00	Xiaoliuqiu	1.09	4.2	4.3	168	14.7	12.0	173	Summer monsoon
#9	2014/11/02 19:00	Longdong	2.05	5.7	8.2	56	20.7	15.3	17	Typhoon (Nuri)

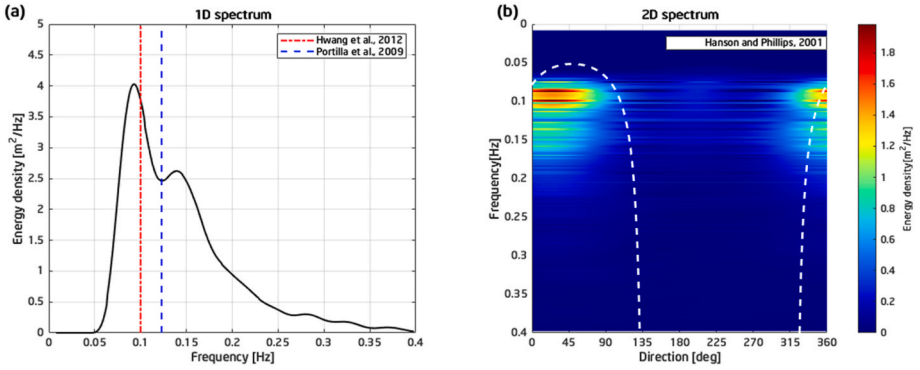

Fig. 3. Example highlighting different identifications in wind sea and swell separation methods: (a) 1D spectrum using the PM peak method (Portilla et al., 2009) with a blue dashed line and the spectrum integration method (Hwang et al., 2012) with a red dashed line; (b) 2D spectrum using the wave age method (Hanson and Phillips, 2001) with a white dashed line. (For interpretation of the references to colour in this figure legend, the reader is referred to the Web version of this article.)

are identified as wind sea, which differs in classification from the two 1D methods. The calibration parameter β is known to influence the range of the wave age parabola, which may affect the identification of the wind sea and swell separation method. Based on suggestions from the literature and our own experience, we use $\beta = 1.5$ for the wave age method. The current setting performs well under general conditions, but under

strong wind conditions, the wave age method may overestimate wind sea energy. Next, we will examine this issue with 9 selected directional wave spectra.

By applying the 2D wave age method on 9 selected directional spectra, the wind sea and swell separation results are shown in Fig. 4. It can be observed that the parabola from the wave age method produces unexpected results when separating wave systems. Two unexpected results are noticed: (1) The wind sea and swell systems are both included within the wave age parabola, as seen in records 1, 2, 4, 6, 7, 8, and 9, corresponding to (a), (b), (d), (f), (g), (h), and (i) in Fig. 4. (2) The deviation of the direction between wind and wind sea leads to the exclusion of wind sea component from wave age parabola, as seen in records 3 and 5, corresponding to (c) and (e) in Fig. 4. The first limitation is that the wave age parabola covers all wind sea and swell components. The wind sea area under the wave age curve is mainly related to the calibration factor β and wind speed. Chen et al. (2015) indicated that the factor β may result in significant differences identification of wind sea and swell. Additionally, researchers use different values of factor β based on their own observation data to fit the local environmental conditions. It is questionable whether a single value of β can accurately determine the energy of wind sea and swell under different atmospheric conditions. For example, in our case, typhoons and monsoons may both produce high wind speeds, however, the resulting sea states can be quite different. Meanwhile, wind speed is also a decisive parameter in determining the range of the wave age parabola in the directional spectrum. The wave age method might overestimate the wind sea under relatively strong wind conditions, where the swell is also included within the wave age parabola. The reason for this may be that achieving a fully developed sea at higher wind speeds is challenging due to the requirement of a longer fetch or sufficient duration, which will be discussed in more detail in the next section. Take the spectrum in record 9, for example, it consists of both wind sea generated by local winds and swell caused by the distant Typhoon Nuri in the Pacific Ocean. Typhoon Nuri did not influence wind conditions in Taiwan due to its considerable distance and the trajectory of its path far away from the region. The local mean wind speed and direction, generated by the local wind, are 15.3 m/s and 17°, respectively. The strong wind produces a larger area of wind sea from the wave age parabola, encompassing both local wind sea energy and typhoon swell, which leads to an overestimation of wind sea.

The second limitation of the wave age method arises from the deviation of wind direction from wave direction caused by refraction effects, particularly when the buoy measurement is located in nearshore areas. This deviation can lead to the failure of identifying wind sea and swell, as the wave age parabola excludes all wave systems, including wind sea and swell. Here, we present wave and wind data from the Longdong buoy, which has this issue due to its location near the shore. We collected one year of wind and wave data from the Longdong buoy in 2014, and the annual statistical results related to the direction are presented in the rose diagrams in Fig. 5. Fig. 5(a) shows the directional distribution of significant wave height. It can be observed that the prevailing wave direction throughout the year primarily comes from the North, ranging approximately from 270° to 30°. Meanwhile, Fig. 5(b) displays the directional distribution of wind speed, where the wind predominantly comes from two directions: northeast and southwest. This pattern is largely influenced by the seasonal monsoons in Taiwan, with the northeast monsoon occurring during the winter months and the southwest monsoon dominating in the summer. This directional misalignment between wind and waves can result in incorrect separation of wind sea and swell, which needs to be corrected accordingly. In the next section, we present our new method for addressing the aforementioned issues.

5. Proposed 2D separation method based on wave growth theory

5.1. Background of wind wave development theory

As previously discussed, the wave age method can overestimate wind sea energy under strong wind conditions. This overestimation may arise

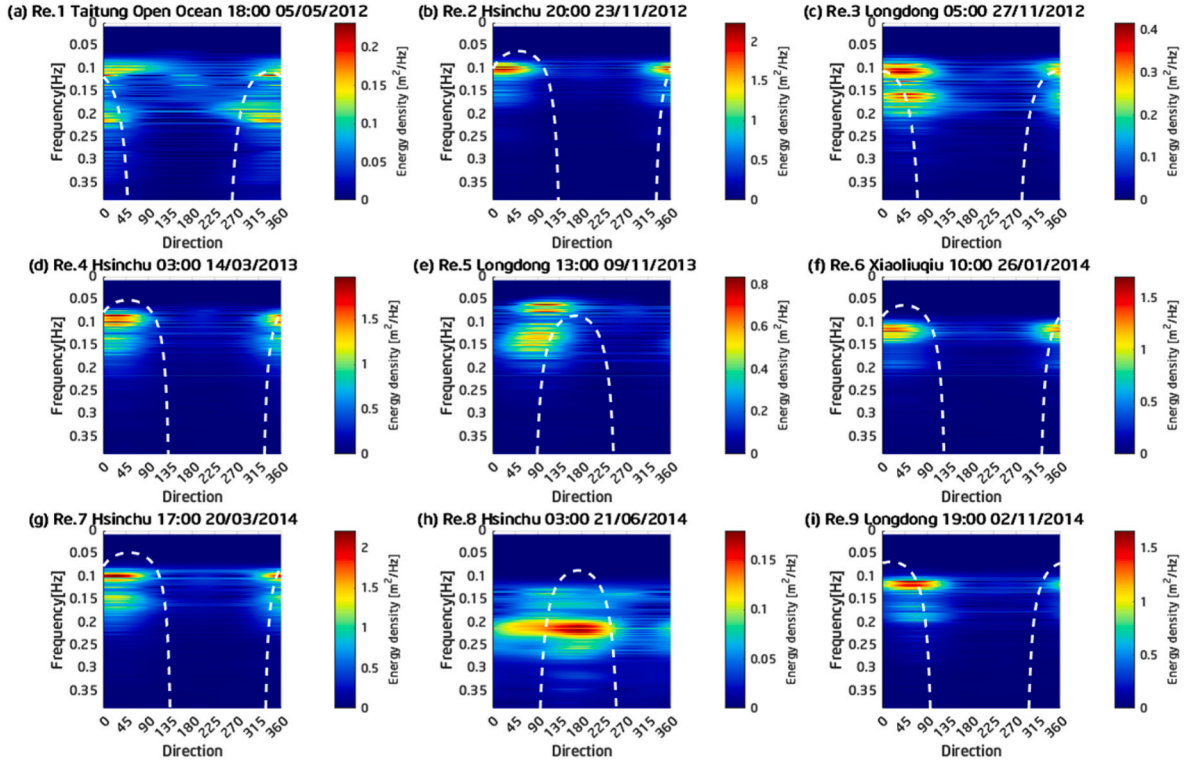

Fig. 4. Wind sea and swell separation results for 9 selected directional wave spectra using the 2D wave age method (Hanson and Phillips, 2001) with white dashed lines.

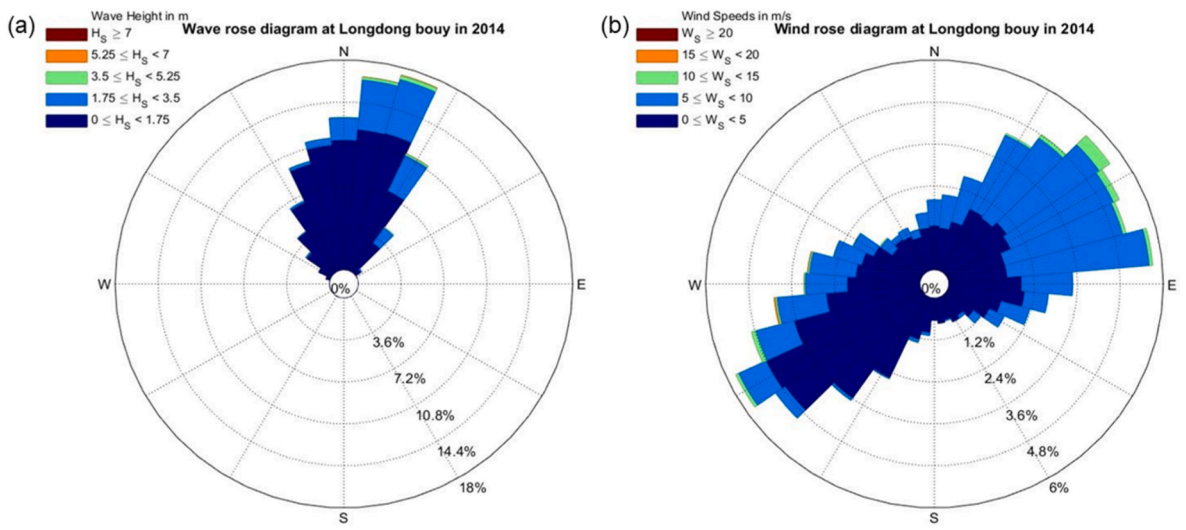

Fig. 5. (a) Rose plot of significant wave height at the Longdong buoy in 2014. (b) Rose plot of wind speed at the Longdong buoy in 2014.

because the local wind-derived wave age parabola may not accurately reflect current wave conditions. To address this limitation, we introduce an additional wind parameter based on wind sea growth theory to improve the existing separation method. The following section provides an overview of wind wave development theory.

Wind sea growth depends on three key factors: wind speed, fetch, and duration. Wind speed drives energy transfer to the ocean surface, fetch determines the spatial range over which waves can form, and duration allows sufficient time for waves to develop. Waseda et al. (2001) demonstrated that changes in wind speed require a response or adjustment period for wind waves to reach equilibrium. Furthermore, Dobson et al. (1989) observed that wind speed varies significantly with fetch in offshore wind conditions. Several studies have shown that wind speed alone is insufficient to accurately describe the growth of wind seas in real sea states. As a result, our study aims to provide valuable insights into wind sea generation processes, enabling an accurate description of wind seas for a new method of wind sea and swell separation.

When a wind blows on the atmospheric boundary layer above the surface, the wind sea grows through the transfer of momentum and energy. The wave generation mechanism, given the specified wind information, is described through spatial and temporal evolutions using fetch-limited growth and duration-limited growth functions. The first research was proposed by Sverdrup and Munk (1947), who combined both field and laboratory data with previous wave theory to obtain semi-empirical wave forecasting relationships. The limit of wave growth corresponding to fully developed seas was reported by Bretschneider (1958) and Pierson and Moskowitz (1964). The fetch-limited wave growth is measured in the restricted lake or sea in large numbers of papers (Sverdrup and Munk, 1947; Bretschneider, 1958; Hasselmann et al., 1973; CERC, 1977; Kahma, 1981; Donelan et al., 1985; Dobson et al., 1989; Donelan et al., 1992; Young, 1999; Hwang and Wang, 2004). It describes the wave generation process in which a steady wind blows perpendicular to a straight shore. Meanwhile, the wind waves grow up in a given fetch during propagation and reach a statistically equilibrium state with unlimited duration.

The case in which the wave development is not affected by the limitation of fetch and spatial homogeneity is referred to as duration-limited wave growth. The duration-limited wind waves are generated from an initially calm sea under the condition that an abrupt increase of wind up to a steady speed occurs over a successive duration. This ideal condition of duration-limited wave growth rarely occurs in nature due to the complex and dynamic variations of local winds. Consequently, the reports of duration-limited wave growth data are only cited by Sverdrup and Munk (1947), Bretschneider (1952a,b), Darbyshire (1959), DeLeonibus and Simpson (1972), CERC (1977), Mitsuyasu and Rikiishi (1978) and Hwang and Wang (2004). Hwang and Wang (2004) established the higher-order fetch-limited and duration limited functions to describe the steeper rate at an early stage of development. Fontaine (2012) showed that relationship between fetch and duration laws was formally interrelated according to wave trains evolution equations by Waseda and Tulin (1999) and Tulin and Waseda (1999). Considering the atmospheric and geographic conditions in Taiwan, the fetch is generally long enough due to the vast expanse of the Pacific Ocean and South China Sea. Given the extensive bodies of water surrounding Taiwan, winds can blow uninterrupted over significant distances. Therefore, in this study, we assume an infinite fetch to approximate the conditions for wave growth, but the duration is limited based on the realistic wind conditions.

The wind sea growth functions describe how wind sea is generated by wind and provide valuable insight into the physical processes of wind sea evolution (Young, 1999). The dimensionless duration-limited wave functions can be obtained from the factors of the non-dimensional wave energy E^*, the non-dimensional angular frequency of the spectral peak Ω^* and the non-dimensional wind duration t^*. The wave growth can be represented by power-law functions:

$$E^* = A_{et} t^{*a_{et}} \tag{6}$$

$$\Omega^* = A_{\omega t} t^{*a_{\omega t}} \tag{7}$$

where $E^* = \sigma^2 g^2 / U^4$, $\Omega^* = U\omega_p / g$, $t^* = gt/U$, σ^2 is variance of surface displacement, ω_p is the peak angular frequency; U is the wind velocity, t is the wind duration and g is the gravitational acceleration, A_{et}, a_{et}, $A_{\omega t}$, $a_{\omega t}$ are the coefficients and exponents determined based on different experiments.

Since the field measurements of duration-limited growth are scarce, the space-time conversion equations are important in order to convert the fetch-limited growth functions into the duration-limited growth functions (Bretschneider, 1952a, 1952b; Mitsuyasu and Rikiishi, 1978; Hwang and Wang, 2004). Following the procedure of space-time conversion in Hwang and Wang (2004), the coefficients and exponents of the duration-limited growth can be calculated from the fetch-limited growth functions. The results from the data of the past studies (Hasselmann et al., 1973; CERC, 1977; Young, 1999; Hwang and Wang, 2004) are shown in Table 3. Different empirical coefficients of wave growth functions are regressed against different experimental or field data. Hasselmann et al. (1973) determined the fetch-limited growth by JONSWAP studies. CERC (1977) summarized the wave growth functions

Table 3
Coefficients and exponents for duration-limited wave growth functions.

Reference	A_{et}	a_{et}	$A_{\omega t}$	$a_{\omega t}$
Hasselmann et al. (1973)	2.23×10^{-10}	1.49	33.94	−0.49
CERC (1977)	3.71×10^{-9}	1.12	14.62	−0.33
Young (1999)	1.14×10^{-8}	1.07	16.97	−0.33
Hwang and Wang (2004)	1.24×10^{-8}	1.07	15.78	−0.32

according to Sverdrup, Munk and Bretschneider empirical functions (SMB) with both laboratory and field data sources. Young (1999) summarized the average wave growth laws by using all previous field data. Hwang and Wang (2004) carried out an experiment in St. Andrew Bay near Florida to get the wave growth functions for both fetch-limited and duration-limited conditions. Subject to the above quantitative discussions, the coefficients and exponents of duration-limited wave growth functions will be further applied to wind sea and swell separation method.

5.2. A new separation criteria duration-limited wave growth

The duration-limited wave growth functions describe the development of characteristic wave height and wave period as a function of wind speed and duration. Recovering the units from dimensionless form, Eq. (7) becomes:

$$\frac{U\omega_p}{g} = A_{\omega t}\left(\frac{gt}{U}\right)^{a_{\omega t}} \tag{8}$$

To obtain the peak frequency of wind sea, Eq. (8) is rearranged as:

$$f_p = A_{\omega t}\cdot(2\pi)^{-1}\cdot g^{1+a_{\omega t}}\cdot t^{a_{\omega t}}\cdot \mathrm{U}^{-(1+a_{\omega t})} \tag{9}$$

The peak frequency of wind sea can be determined from wind duration and wind speed, providing a more detailed physical understanding of the wave generation process, as shown in Fig. 6. The value of the curves represented the peak period of the wind-generated sea. The dashed line represented the maximum condition of a fully developed sea, where wind waves have reached their equilibrium state for a given wind speed and duration. This ensures that the peak period does not exceed the maximum value within the equilibrium range of air-sea interaction. Overall, this figure illustrates how both wind speed and duration influence the development of wind sea, with higher wind speeds and longer durations resulting in longer wave periods.

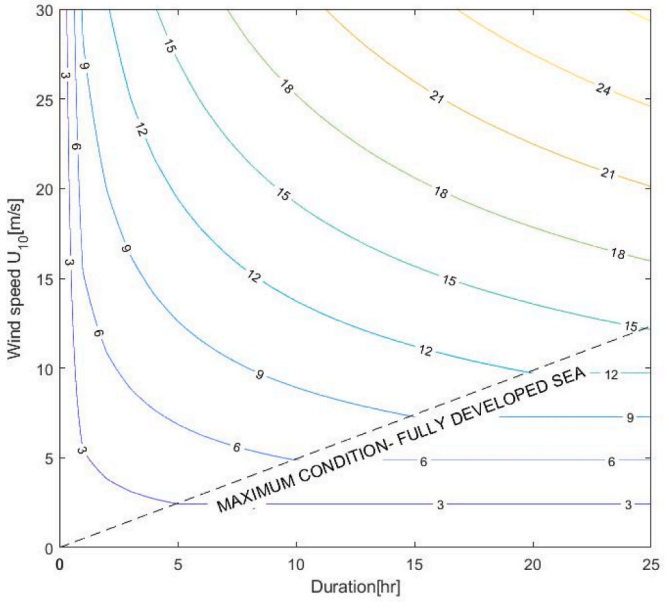

Fig. 6. Wind sea growth contours relating wind speed, duration, and wave peak period.

To obtain the separation frequency, the peak frequency of wind sea must be multiplied by an empirically determined constant C, which adjusts the peak frequency of wind sea due to environmental influences (Earle, 1984; Vartdal and Barstow, 1987; Gilhousen and Hervey, 2001). However, the spatially homogeneous duration-limited growth functions derived from steady wind fields are not entirely consistent with realistic field environments (Romero and Melville, 2010; Hwang et al., 2011). We consequently give a new calibration constant β_s in accordance with the past studies on wave growth to adjust the gap between peak frequency of wind sea and separation frequency,

$$\beta_s = \mathrm{C}\cdot A_{\omega t}\cdot(2\pi)^{-1}\cdot g^{1+a_{\omega t}} \tag{10}$$

In this study, we use the coefficients of Hasselmann et al. (1973), as shown in Table 3. The constant C is similar to the calibration factor β to include all wind sea components in the parabolic region. The constant C is set as 6.2 based on our empirical estimation by our data, and obtained β_s is equal to 106.7.

The wind direction makes a great difference in this identification criterion. Ideally, the direction of local wind sea varies depending on the direction of the wind. Hanson and Phillips (2001) classified the spectral components as wind sea if their direction is within plus-minus 90° of the prevailing wind direction. This identification of wind sea propagation direction is defined as:

$$|\theta - \psi| < \frac{\pi}{2} \tag{11}$$

where θ is the wave direction and ψ is the wind direction. Combining Eq. (9), Eq. (10) and Eq. (11), the new criteria to identify wind sea and swell becomes:

$$f_s = \beta_s\, t^{a_{\omega t}}\left(U\cos(\theta-\psi)\right)^{-(1+a_{\omega t})} \tag{12}$$

This equation defines a parabolic region in the frequency-direction domain, and the wind sea partitions are those whose peaks fall within the parabolic region. Under a constant wind speed condition, the range of the parabolic region increases with the gradually accumulated wind duration. The wave growth eventually reaches its limit, transitioning to a fully developed state, and this maximum parabola produces the same region as the wave age method.

We provide an example of the new criteria based on duration-limited wave growth for a case with a wind speed of 10 m/s, as shown in Fig. 7. The different wave age parabolas correspond to various durations, specifically 1 h (blue), 3 h (orange), 5 h (yellow), 10 h (purple), and the maximum duration of 20 h (black). It can be observed that under a steady wind speed, as the duration increases, the range of the wave age parabola becomes larger, allowing it to include longer waves. In the following, we will discuss how we determine the wind duration.

5.3. Determination of wind duration

Determination of wind duration is necessary in the wind sea and swell separation process to determine how long the wind has been blowing at a constant speed and direction. This stationarity of wind field in the wave growth assumption rarely existed in the real open ocean (Hwang and Wang, 2004). Various studies have proved that the wave growth functions can be applied in unsteady wind conditions (Young, 2006; Romero and Melville, 2010; Hwang et al., 2011; Young and Vinoth, 2013; Hwang, 2016). The wave growth functions can be applied by three different scaling wind velocities such as the wind speed at 10 m elevation U_{10}, the wind friction velocity u_* and the wind velocity at an elevation equal to one-half of the characteristic wavelength $U_{\lambda/2}$ (Hwang, 2006). This study adopts U_{10} as the reference wind velocity,

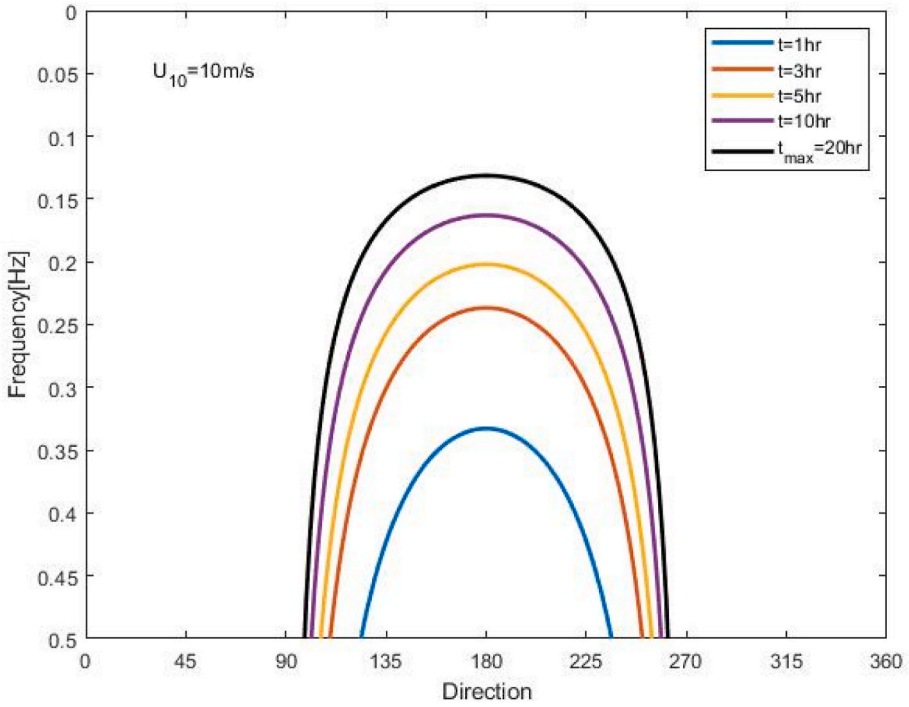

Fig. 7. Illustration of new developed criterion for wind sea and swell separation in the frequency-direction domain under the wind speed $U_{10} = 10$ m/s for different values of wind duration.

following a widely accepted convention with the advantages of standardization and comparability in ocean engineering and oceanography.

To retrieve the effective wind duration, we need to remove unstable wind conditions from the measured data, thereby avoiding the miscalculation of wind sea and swell separation. This idea originates from the concept of wave response time, which describes how waves obtain energy from changing wind conditions (Hasselmann et al., 1976). The directional response due to the mean wave direction lagging behind the wind direction in turning wind situations has also been discussed to determine the directional relaxation time, which is widely considered in wave modeling (Günther et al., 1981; Van Vledder and Holthuijsen, 1993; Quanduo and Komen, 1993). Mahrt (2011) found that weak winds caused common large shifts in wind direction, and wind direction variability increased rapidly for wind speeds less than 2 m/s at a 2 m elevation. As regards the steady wind direction, the allowable ranges vary among ±20° (Kahma, 1981; Ardhuin et al., 2007) or ±30° (Hasselmann et al., 1973; Donelan et al., 1992) of the mean wind direction. In this study, three criteria are proposed to estimate the effective wind duration from time series of field wind measurements.

1. Weak wind conditions are defined as wind speeds below 3.5 m/s. Under such conditions, the wind duration is initialized to a background value and does not accumulate over time.
2. Once wind duration begins to accumulate, the mean wind direction must remain within ±30° relative to the mean wind direction recorded 1 h earlier, ensuring directional consistency.
3. The maximum wind duration is constrained by the condition of a fully developed sea, as defined by Pierson and Moskowitz (1964).

$$t^*_{max} = 7.15 \times 10^4 \tag{13}$$

Here, t^*_{max} is a dimensionless parameter. This parameter represents the duration limit at which the wind sea reaches a fully developed state. It can be calculated by combining $\Omega^* = 0.8$ (Young, 1999; Hwang, 2016) with duration-limited growth functions. The coefficients for duration-limited growth are referenced from Hwang and Wang (2004), as shown in Table 3. When applying the coefficients to our dataset, we found they did not adequately describe our data. This discrepancy may be attributed to the Pacific Ocean and the East China Sea, which provide a larger fetch and duration for the generation of larger waves. Therefore, the maximum wind duration should be longer for our data than the initially obtained value, and we derived the final maximum wind duration through empirical adjustments. For weak wind conditions with a mean wind speed of 3.5 m/s, the maximum wind duration is approximately 7 h; we set this duration as the initial value. The above criteria to approximate the effective duration are based on our own empirical design. It is worth noting that different sea states exhibit distinct wind and wave characteristics, which can vary significantly across geographic locations due to local environmental and climatic conditions.

5.4. Extending to nearshore data

When a train of waves propagates into shallow water, it is well known that its velocity and wavelength decrease, and the direction of the crests changes to become nearly parallel to the shore (Longuet-Higgins, 1957). The main wave direction measured by the nearshore buoy is normally inconsistent with the prevailing wind direction due to the wave refraction induced by changes in the nearshore bathymetry. Consequently, winds and propagating waves occur to some extent from different directions (Donelan et al., 1985; Arndt et al., 2019). This directional misalignment will result in incorrect separation of wind sea and swell.

If wave diffraction effects are neglected, the relationship between a spatially homogeneous incident wave spectrum and a spectrum in shallow water was proposed by Longuet-Higgins (1957). They showed that the ray equation can be applied to spectra and that the relationship between the initially undisturbed spectrum E_0 and refracted spectra E is described by:

$$E(f,\theta) = \frac{k}{k_0}\frac{C_{g0}}{C_g}E_0(f, \Gamma(f,\theta)) \tag{14}$$

where C_{g0} is the initial group velocity, C_g is the refracted group velocity, k is the wave number, and k_0 is the initial wave number. The inverse

direction function Γ describes the frequency-dependent relationship between the initial and refracted wave direction, where $\theta_0 = \Gamma(f,\theta)$. The initial direction θ_0 corresponds to the wave's propagation angle in deep water at an offshore location before interacting with varying bathymetry. This inverse direction function is obtained by ray equations following Snell's law when phase speed varies above bathymetry (Munk and Arthur, 1952; Dobson, 1967).

We now illustrate how to revise this directional misalignment based on our field measurement data. We assume that the wind sea direction in offshore aligns with the direction of the wind responsible for its generation, which can be expressed by $\theta_0 = \psi$. The refracted wave direction is determined using wave rays and is expressed as $\theta = \Gamma^{-1}(\theta_0)$. Based on the above, the change in angle between the offshore wind-generated wave direction and the nearshore arrival angle can be calculated:

$$\Delta\psi = \left|\Gamma^{-1}(\psi) - \psi\right| \tag{15}$$

The change in angle between the offshore wind-generated wave direction and the nearshore arrival angle is incorporated into the wind sea and swell separation method to enhance the identification of nearshore data. The angular adjustment to Eq. (12) can be expressed as

$$f_s = \beta_s\, t^{a_{ot}} \left(Ucos(\theta - \psi \pm \Delta\psi)\right)^{-(1+a_{ot})} \tag{16}$$

By accounting for this angular adjustment, the method ensures that the wind direction aligns with the refracted wind sea and is distinguished based on its local long-term statistics. This correction reduces directional misalignment, leading to more reliable separation of wind sea and swell components in nearshore environments.

6. Results

6.1. Applying the proposed method to 9 wave spectra

In this section, we apply our proposed wind sea and swell separation method to 9 selected wave spectra and compare the results with those obtained using the wave age method, as shown in Fig. 8. Before identifying wind sea and swell using our proposed method, the 2D spectral partitioning technique by Portilla et al. (2009) is applied to our directional spectra to remove spurious partitions. A convolution kernel is used to smooth the directional spectrum, leaving only the significant spectral components. After partitioning, our proposed method is then applied to classify these spectral partitions as wind sea or swell. In Fig. 8, the parabola derived from the duration-limited growth method is represented by the red line, while the wave age method is shown with the dashed white line. Considering wind speed and duration, the separation results, including significant wave height, mean periods, peak periods, and main direction for both wind sea and swell, are presented in Table 4. The sub-indexes s and w indicate the swell and wind sea, respectively. The direction difference ($\Delta\theta$) between swell direction and wind sea direction is also calculated. The dimensionless parameter sea-swell energy ratio ($SSER = E_s/E_w$) is used to present the dominance of the sea states between swell and wind sea (Guedes Soares, 1984). This parameter $SSER$ can divide wave spectra into three cases: swell-dominated ($SSER < 1$); wind sea dominated ($SSER > 1$) and sea-swell energy comparable ($SSER \approx 1$). In the selected spectra, records 1, 2, 4, 6, 7, 8, and 9 exhibit an overestimation of wind sea due to the inclusion of swell components within the wave age parabola. Based on the Beaufort wind force scale, wind speeds from 0 to 8 m/s (Beaufort 0–4) are classified as small wind conditions. Moderate wind conditions range from 8 to 13 m/s (Beaufort 5–6), and wind speeds above 13 m/s (Beaufort 7+) are considered strong wind conditions. In our records, 1, 3, 5, and 8 correspond to moderate wind speeds, while the others represent stronger wind speeds. Under small or moderate wind speeds, it is easier to reach the maximum duration for fully developed seas compared to strong wind speeds. This can be observed in Table 4, where larger mean wind speeds correspond to longer maximum durations, as calculated using Eq. (13). By considering wind duration, it can be observed that the new parabola has a smaller range than the one by the wave age method. The new method successfully separates wind sea and swell in records 1, 2, 4, 6, 7,

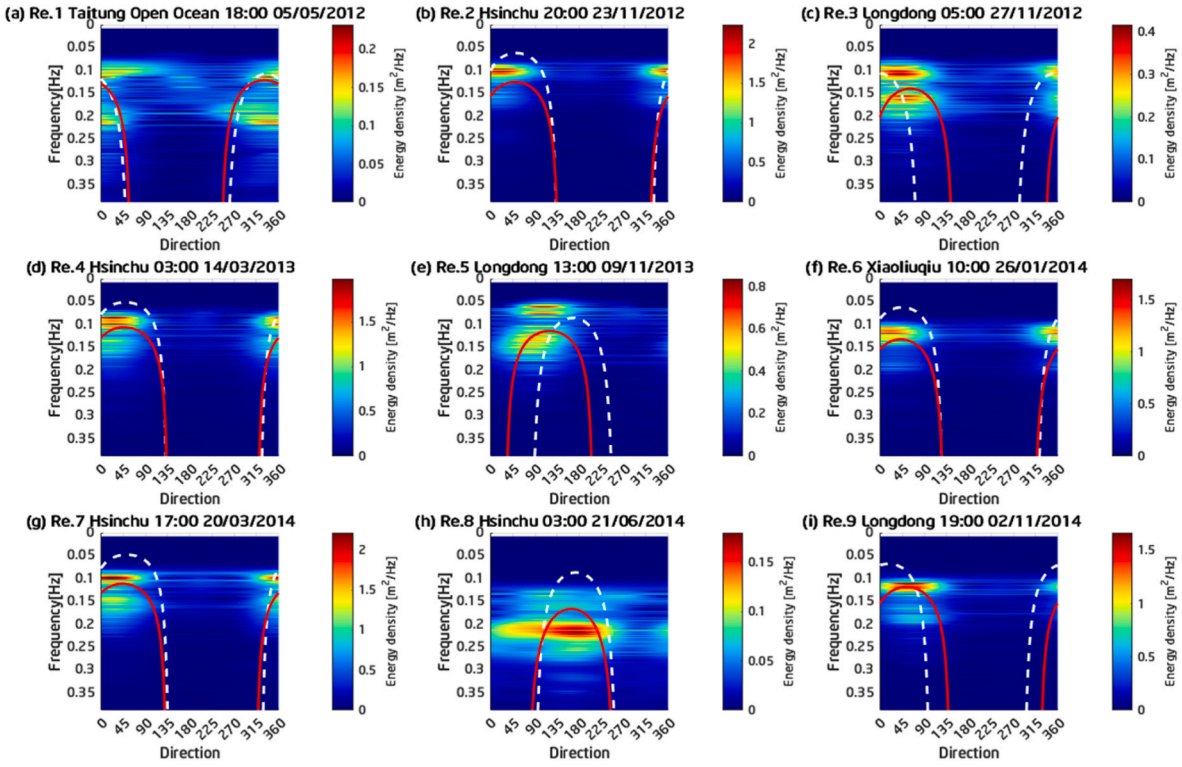

Fig. 8. Separation results of wind sea and swell by proposed Duration-limited growth method (red solid line) and Hanson and Philips (2001)'s wave age parabola method (white dashed line). (For interpretation of the references to colour in this figure legend, the reader is referred to the Web version of this article.)

Table 4
Separation results by proposed duration-limited growth method.

No.	U_{mean}(m/s)	t (hr)	t_{max} (hr)	Swell				Wind sea				Δθ(°)	SSER (Es/Ew)	Dominance
				H_{m0s}(m)	T_{ps}(s)	T_{m02s}(s)	θ_s(°)	H_{m0w}(m)	T_{pw}(s)	T_{m02w}(s)	θ_w(°)			
#1	9.6	19	20	0.65	9.8	9.3	30	0.90	4.7	4.3	344	46	0.52	wind sea
#2	16.7	15	34	1.82	9.8	9.0	18	1.40	6.3	4.8	7	11	1.69	swell
#3	9.8	19	20	0.89	9.5	8.3	39	1.06	6.3	4.8	49	10	0.70	wind sea
#4	20.2	16	41	1.72	11.4	9.7	24	1.75	7.4	5.2	15	9	0.97	sea-swell mixing
#5	12.1	24	25	1.05	16.4	11.0	108	1.41	7.5	5.7	89	19	0.55	wind sea
#6	16.6	15	34	1.69	9.0	8.0	16	1.11	5.3	4.4	25	9	2.32	swell
#7	21.6	19	44	1.71	10.2	9.7	21	2.04	6.9	5.3	22	1	0.70	wind sea
#8	12.0	14	24	0.60	7.2	5.4	112	0.92	4.6	4.1	172	60	0.43	wind sea
#9	15.3	26	31	1.55	8.9	7.9	60	1.41	5.4	4.8	70	10	1.21	sea-swell mixing

8, and 9 under moderate and strong wind conditions.

As mentioned in Section 4, the buoy measurements located nearshore may result in incorrect identification of wind sea and swell due to refraction effects. Records 3, 5, and 9 were collected from the Longdong buoy, with records 3 and 5 exhibiting this issue. Using Eq. (15), the angle adjustment $\Delta\psi$ between wind and incident wind sea is 56° for record 3 and 44° for record 5, respectively. With this angle adjustment, it can be observed that the vertex direction of the parabola in the proposed method has been modified compared to the wave age method, aligning more closely with the wind sea direction. This adjustment leads to more accurate separation of wind sea and swell. Our results demonstrate that the proposed method is applicable to data collected from nearshore buoys or sites significantly influenced by refraction or diffraction.

Finally, we investigate whether our wind sea components exhibit wind wave characteristics that conform to the wind sea growth function. The function was established based on the saturated sea conditions that characterize the local wind-generated wave system. Hwang et al. (1998) simplifies the wave growth function by eliminating the fetch parameter, and the resulting equation is

$$\left(\frac{U_{10}}{gT_p}\right) = 4.8 \times 10^{-2} \left(\frac{U_{10}^2}{gH_s}\right)^{2/3} \tag{17}$$

where T_p is the peak period and H_s is the significant wave height. This wind sea function can accurately describe the data from the North Sea, as measured by JONSWAP (Hasselmann et al., 1973, 1976; Toba, 1978), and the Gulf of Mexico (Hwang et al., 1998). Based on our wind sea and swell separation results using the duration-limited growth method, we compare the wind sea function with the components of wind sea and swell of 9 selected spectra, as shown in Fig. 9. It is found that the wind wave data are closer to this function, while the swells deviate more from it. This result demonstrates that our method is effective in separating wind sea and swell.

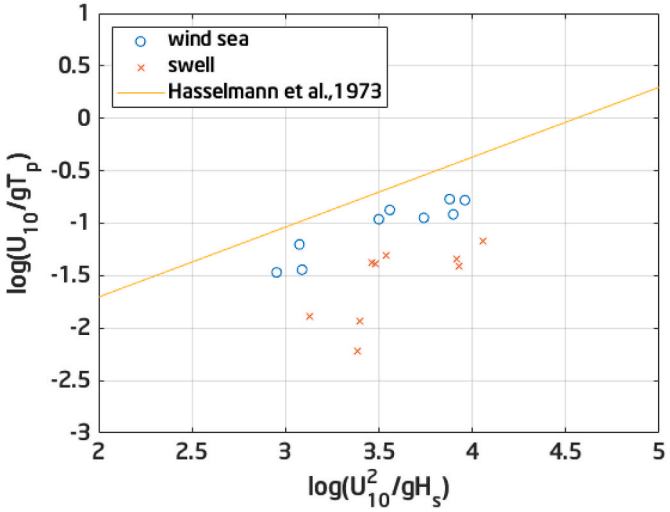

Fig. 9. The scatterplot of log (U/gT_p) and log (U^2/gH_s) for wind sea and swell separation results using duration-limited growth method.

6.2. Applying the proposed method to a case study

In this section, we present a case study from May 4 to May 7, 2012, collected by the Taitung Open Ocean buoy. Record 1 is one of the spectra in this case study. Fig. 10 shows the surface pressure map at 12:00 on May 4 and 12:00 on May 5 to illustrate the meteorological conditions. The spring weather in Taiwan was sometimes influenced by the winter monsoon, which is produced by the movement of the atmospheric low pressure in East Asian. Before the day of 4 May, the cold front had passed through the East Sea. After 24 h, the low-pressure system over Japan continued to move northeast, and the high-pressure area from China moved eastward. These meteorological conditions determine the wind field and wave field, which are shown in Fig. 11. The time series of wave and wind data includes significant wave height, wave period, wind speed U_{10}, wind direction, and wave direction. Wave height started to develop after the afternoon of May 4 and reached a maximum value of 1.36 m at noon on May 5. The mean period was about 5 s at all times during the observation, but the high peak period of up to 8 s revealed the presence of swell energy from far away. The main wind direction on May 4 was from the south, but on May 5, the wind direction shifted to the north, and the wind speed increased from 3.6 m/s to 14.8 m/s. This explained the condition of wind sea and swell coexistence, where the wind sea began to develop as the wind turned north, and simultaneously, swell arrived from the north due to the northeast monsoon.

Fig. 12 illustrates the separation results obtained using the duration-limited method and the wave age method in the frequency domain over the entire analyzed period. The separation frequency produced by the wave age method is shown as a black dashed line, while that from the duration-limited growth method is represented by a red line. It can be observed that low-frequency swell energy persisted throughout the entire period, while on May 5, high-frequency wind sea energy emerged with the increasing wind speed. The separation result obtained by the Hanson and Phillips (2001) method includes the swell energy in the wind sea component, resulting in an overestimation of wind sea. This separation problem occurred because the local wind cannot immediately generate wind waves that satisfy the fully developed condition at the corresponding frequency. This method uses wave age as a separation criterion when it satisfies the condition of a fully developed sea. In other words, wave age can only determine one condition of sea state, and it cannot describe the process of wind wave growth and evolution. Regarding the duration-limited growth method employed in this study, the two wave systems can be successfully separated into wind seas and swells. Note that the variation of separation frequency of the duration-limited growth method on May 5 gradually decreased with the growing wind speed and the accumulation of wind duration. This result illustrates the advantage of this method, which optimizes the efficient utilization of the wind information to describe the complex processes of wind sea generation.

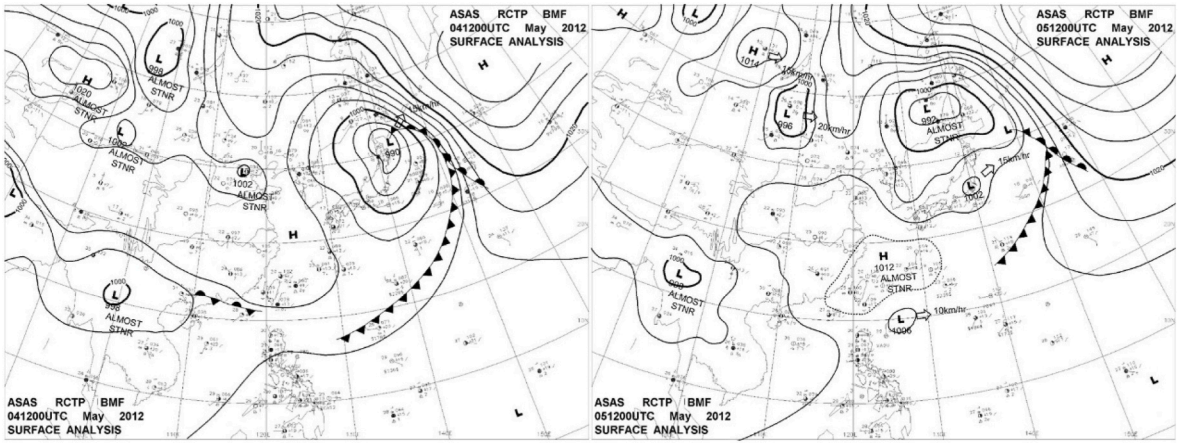

Fig. 10. Surface pressure map at 12:00 on May 4 and 12:00 on May 5, 2012.

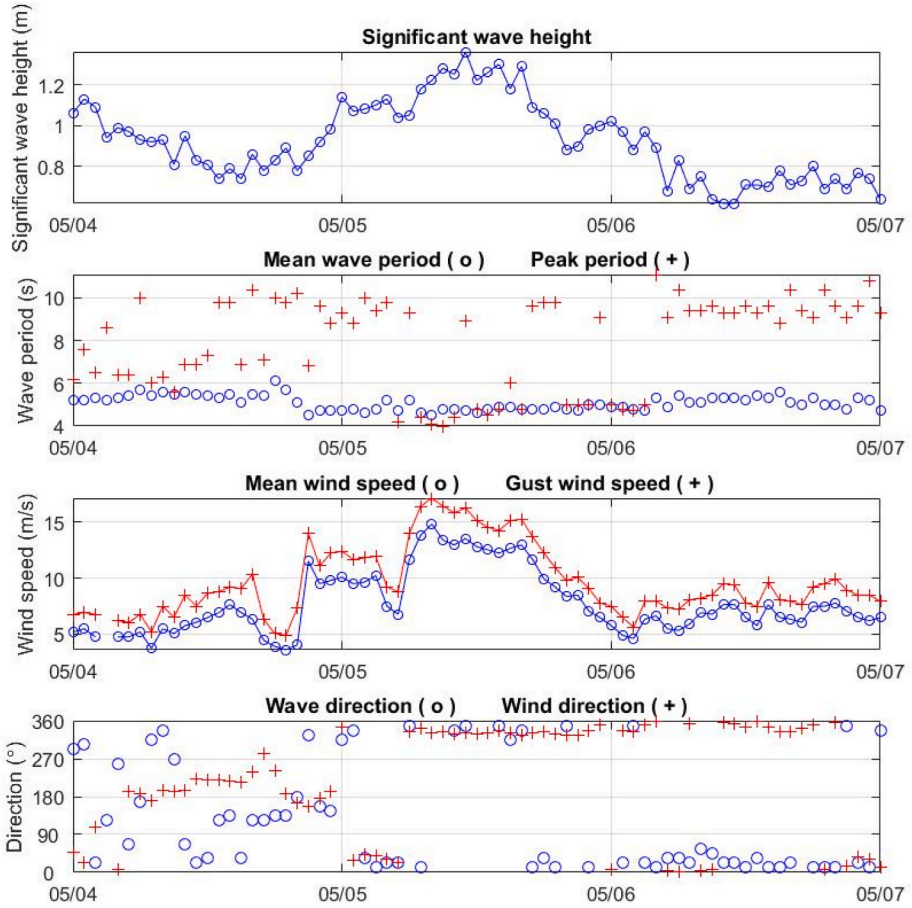

Fig. 11. The times series of (a) significant wave height, (b) mean wave period (circles) and peak wave period (crosses), (c) mean wind speed (circles) and gust wind speed (crosses), (d) wind direction (circles) and wind direction (crosses) during winter monsoon period from May 4 to May 7 in year 2012 measured by Taitung Open Ocean buoy.

Meanwhile, it can be noted that at the beginning of May 6, the wind speed started to decrease, which caused the identification of an old wind-sea as a young swell. So far, existing wind-sea and swell separation methods have been unable to effectively handle the transformation of wind-seas into swells when the wind speed suddenly decreases or the wind direction abruptly changes. Accurate separation of wind sea and swell is difficult because the transition between wind sea and swell is not well-defined. Further investigation is required to address these transition scenarios better.

To illustrate the distinct characteristics of wind sea and swell, wave steepness is used as an important comparative parameter. Wave steepness is defined as the ratio of wave height to wavelength, which is widely used to describe basic wave information, particularly in relation to nonlinear processes such as wave grouping, whitecapping, and wave breaking. The wave steepness can be expressed as

$$S = \frac{2\pi H_s}{g T_p^{\,2}} \tag{18}$$

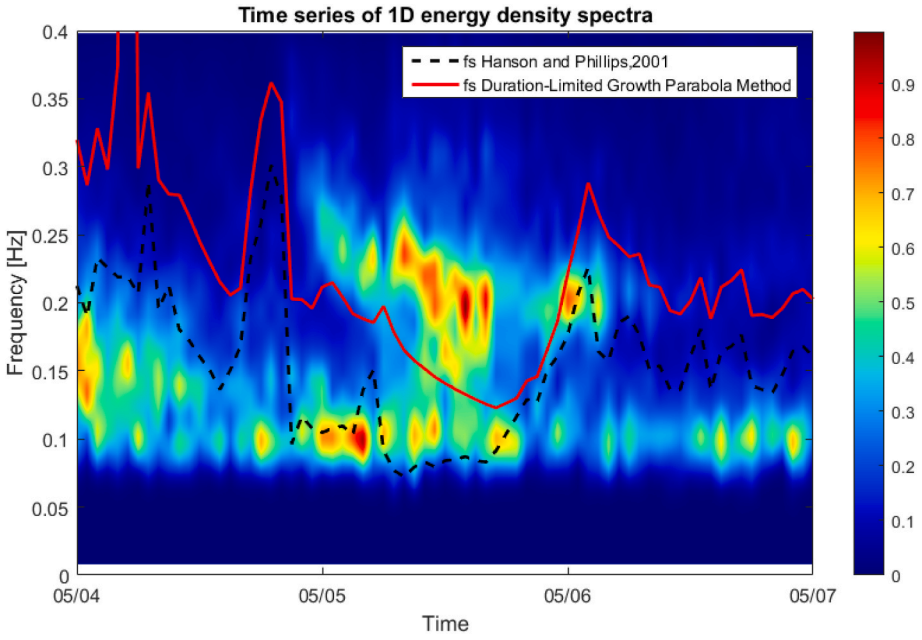

Fig. 12. The time series of energy density spectra with wind sea and swell.

where g is gravitational acceleration, H_s is the significant wave height and T_p is the peak period. Generally, wind seas have a higher wave steepness than swells. Fig. 13 shows the steepness results for the wind sea and swell components separated using the proposed method. The dark orange line represents the steepness limit, indicating that the waves grow in height and will reach their maximum height and breaking point. Toffoli et al. (2010) combined the laboratory data and field data on wave breaking. They found that front-face wave steepness rises up to the threshold value of $kH/2 = 0.55$, where the wave number $k = 2\pi/L$. The separation results clearly show three clusters based on the duration-limited growth method, with the black triangles representing the raw data, the blue circles representing wind sea and red crosses representing swell. The wind sea data exhibit a positive correlation between wave height and length, whereas the swell data appear relatively scattered and trendless. This result confirms that our proposed method can produce reasonable and consistent outcomes for the separation of wind sea and swell.

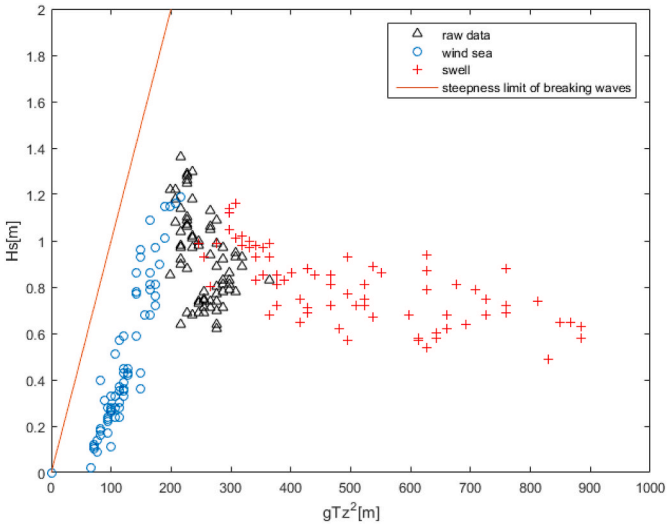

Fig. 13. Scatter diagram of wave steepness for wind sea (circles), swell (crosses) and raw data (triangles).

7. Conclusions

In the open ocean, wave spectra often display two or more spectral peaks due to the coexistence of locally generated wind waves and swells originating from distant weather systems. Separating wind sea and swell components is crucial for advancing research on wave dynamics, improving wave forecasting, and supporting practical engineering applications. The wave age method for two-dimensional wind sea and swell separation was evaluated using wind and wave data collected from buoy stations around Taiwan. It was found that the wave age method may produce unexpected results when analyzing bimodal spectra: (1) The wind sea and swell systems may be both included within the wave age parabola under moderate or strong wind speed conditions. (2) The directional deviation between the wind and wind sea causes the exclusion of the wind sea component from the wave age parabola. The wave age method led to the aforementioned problems because it is based on the assumption of fully developed seas and does not consider the refraction effect.

Our study proposes a new method for separating wind sea and swell based on duration-limited growth, which enables a more precise description of wind sea during the wind wave growth process and covers a wider range of wave development stages. The cases of duration-limited growth assumed an infinite fetch, meaning there were no boundary limitations for wave growth. Wind duration was a new parameter used for the first time in the 2D wind sea and swell separation method. Using the duration-limited growth function and an empirically-determined constant, a new separation criterion in Eq. (12) was proposed. Meanwhile, this method also accounts for directional misalignment in nearshore areas to address the issue of wave refraction effects. We selected 9 directional wave spectra collected by buoys in Taiwan waters, covering the dominant marine weather phenomena in Taiwan waters, including monsoons and typhoons. These 9 selected spectra exhibited the abovementioned issues. Our proposed method, considering duration-limited wave growth, effectively addresses these issues. The separation results demonstrate distinct wave characteristics of wind sea and swell, with the wind sea exhibiting characteristics consistent with the power law of wind-generated waves. A case study also demonstrates the sensible results. The calibration parameter β_s in our proposed method is empirical and may exhibit variability across different sea states. Further research involving a more extensive dataset is recommended to assess the validity

and establish the generalizability. Additionally, our proposed method is based on an assumption derived from the deep-water dispersion relationship, whereas the effects of finite water depth can be further explored in future studies.

CRediT authorship contribution statement

Yu-Chen Lee: Writing – original draft, Validation, Software, Project administration, Methodology, Investigation, Formal analysis, Data curation. **Dong-Jiing Doong:** Writing – review & editing, Validation, Supervision, Project administration, Methodology, Funding acquisition, Data curation, Conceptualization.

Declaration of competing interest

The authors declare that they have no known competing financial interests or personal relationships that could have appeared to influence the work reported in this paper.

Acknowledgements

This research was jointly supported by the Central Weather Administration (Project No. MOTC-CWA-114-O-02) and the National Science and Technology Council (Project No. MOST 110-2221-E-006-072-MY3) of Taiwan. The authors sincerely thank both agencies for their generous support, without which this work would not have been possible. The authors would also like to express their sincere appreciation to the three anonymous reviewers for their valuable and constructive comments during the review process. Their insightful suggestions greatly improved the quality and clarity of this manuscript.

References

Ardhuin, F., Herbers, T.H.C., Watts, K.P., van Vledder, G.P., Jensen, R., Graber, H.C., 2007. Swell and slanting-fetch effects on wind wave growth. J. Phys. Oceanogr. 37, 908–931.
Ardhuin, F., Sutherland, P., Doble, M., Wadhams, P., 2016. Ocean waves across the Arctic: attenuation due to dissipation dominates over scattering for periods longer than 19 s. Geophys. Res. Lett. 43 (11), 5775–5783.
Arndt, H., Boso, S., Steffen, M., 2019. Wind-wave misalignment and a combination method for direction-dependent extreme incidents. Ocean Eng. 180, 10–22.
Bidlot, J.R., 2001. ECMWF wave-model products. In: ECMWF Newsletter, 91. ECMWF, Reading, United Kingdom, pp. 9–15.
Bretschneider, C.L., 1952a. Revised wave forecasting relationship. Proc. 2nd Conf. on Coastal Engineering. Council on Wave Research, Houston, TX, ASCE.
Bretschneider, C.L., 1952b. The generation and decay of wind waves in deep water. Trans. Am. Geophys. Union 33, 381–389.
Bretschneider, C.L., 1958. Revised wave forecasting relationships. Proc. 6th Conference on Coastal Engineering. ASCE, pp. 30–67.
CERC, 1977. Shore Protection Manual. U.S. Army Coastal Eng. Res. Cent., Washington, D.C.
Chen, G., Chapron, B., Ezraty, R., Vandemark, D., 2002. A global view of swell and wind sea climate in the ocean by satellite altimeter and scatterometer. J. Atmos. Ocean. Technol. 19 (11), 1849–1859.
Chen, Z., Zhang, L., Zhao, C., et al., 2015. A practical method of extracting wind sea and swell from directional wave spectrum. J. Atmos. Ocean. Technol. 32 (11), 2147–2159.
Darbyshire, J., 1959. Further investigation of wind generated waves. Dtsch. Hydrogr. Z. 12, 1–13.
DeLeonibus, P.S., Simpson, L.S., 1972. Case study of duration-limited wave spectra observed at an open ocean tower. J. Geophys. Res. 77, 4555–4569.
Delpey, M.T., Ardhuin, F., Collard, F., Chapron, B., 2010. Space-time structure of long ocean swell fields. J. Geophys. Res.: Oceans 115 (C12).
Dobson, R.S., 1967. Some Applications of a Digital Computer to Hydraulic Engineering Problems. Stanford Univ., Dept. of Civil Eng., Tech. Rept, No. 80.
Dobson, F., Perrie, W., Toulany, B., 1989. On the deep-water fetch laws for wind-generated surface gravity waves. Atmos.-Ocean 27, 210–236.
Donelan, M.A., Hamilton, J., Hui, W.H., 1985. Directional spectra of windgenerated waves. Phil. Trans. Roy. Soc. Lond. A315, 509–562.
Donelan, M.A., Skafel, M., Graber, H., Liu, P., Schwab, D., Venkatesh, S., 1992. On the growth rate of wind-generated waves. Atmos.-Ocean 30, 457–478.
Doong, D.J., Chen, S.H., Kao, C.C., Lee, B.C., 2007. Data quality check procedures of an operational coastal ocean monitoring network. Ocean Eng. 34, 234–246.
Drennan, W.M., Graber, H.C., Hauser, D., Quentin, C., 2003. On the wave age dependence of wind stress over pure wind seas. J. Geophys. Res. 108, 8062.
Earle, M.D., 1984. Development of algorithms for separation of sea and swell. National Data Buoy Centre Tech. Rep. 53. MEC-87-1.
Ewans, K.C., Bitner-Gregersen, E., Guedes Soares, C., 2006. Estimation of wind-sea and swell components in a bimodal sea state. J. Offshore Mech. Arctic Eng. 128 (4), 265–270.
Fontaine, E., 2012. A theoretical explanation of the fetch- and duration-limited laws. J. Phys. Oceanogr. 43 (2), 233–247.
Gerling, T.W., 1992. Partitioning sequences and arrays of directional ocean wave spectra into component wave systems. J. Atmos. Ocean. Technol. 9, 444–458.
Gilhousen, D.B., Hervey, R., 2001. Improved estimates of swell from moored buoys. Proc. *Fourth Int. Symp.* WAVES 2000. ASCE, Alexandria, VA, pp. 387–393.
Guedes Soares, C., 1991. On the occurrence of double peaked wave spectra. Ocean Eng. 18 (1–2), 167–171.
Guedes Soares, C., Nolasco, M.C., 1992. Spectral Modeling of Sea States with Multiple Wave Systems, pp. 278–284.
Günther, H., Rosenthal, W., Dunckel, M., 1981. The response of surface gravity waves to changing wind direction. J. Phys. Oceanogr. 11 (5), 718–728.
Hanson, J.L., Phillips, O.M., 2001. Automated analysis of ocean surface directional wave spectra. J. Atmos. Ocean. Technol. 18, 277–293.
Hasselmann, K., Barnett, T.P., Bouws, E., Carlson, H., Cartwright, D.E., Enke, K., Ewing, J.A., Gienapp, H., Hasselmann, D.E., Kruseman, P., Meerburg, A., Müller, P., Olbers, D.J., Richter, K., Sell, W., Walden, H., 1973. Measurements of wind-wave growth and swell decay during the joint north sea wave project (JONSWAP). Dtsch. Hydrogr. Z. 12 (Suppl. A8), 1–95.
Hasselmann, K., Ross, D.B., Miller, P., Sell, W., 1976. A parametric wave prediction model. d. Phys. Oceanogr. 6, 200–228.
Hasselmann, S., Brüning, C., Hasselmann, K., Heimbach, P., 1996. An improved algorithm for the retrieval of ocean wave spectra from synthetic aperture radar image spectra. J. Geophys. Res. 101, 16615–16629.
Hisaki, Y., 2023. Swell and wind-wave height variability in the East China Sea. Ocean Dyn. 73 (8), 493–515.
Hsu, S.A., et al., 1994. Determining the power-law wind-profile exponent under near-neutral stability conditions at sea. J. Appl. Meteorol. 33, 757–765.
Hwang, P.A., 2006. Duration- and fetch-limited growth functions of wind-generated waves parameterized with three different scaling wind velocities. J. Geophys. Res. 111, C02005.
Hwang, P.A., 2016. Fetch- and duration-limited nature of surface wave growth inside tropical cyclones: with applications to air-sea exchange and remote sensing. J. Phys. Oceanogr. 46 (1), 41–56.
Hwang, P.A., Wang, D.W., 2004. Field measurements of duration-limited growth of wind-generated ocean surface waves at young stage of development. J. Phys. Oceanogr. 34, 2316–2326.
Hwang, P.A., Teague, W.J., Jacobs, G.A., Wang, D.W., 1998. A statistical comparison of wind speed, wave height, and wave period from satellite altimeters and ocean buoys in the Gulf of Mexico region. J. Geophys. Res. 103, 10451–10468.
Hwang, P.A., García-Nava, H., Ocampo-Torres, F.J., 2011. Observations of wind wave development in mixed seas and unsteady wind forcing. J. Phys. Oceanogr. 41, 2343–2362.
Hwang, P.A., Ocampo-Torres, F.J., García-Nava, H., 2012. Wind sea and swell separation of 1D wave spectrum by a spectrum integration method. J. Atmos. Ocean. Technol. 29 (1), 116–128.
Jiang, H., Chen, G., 2013. A global view on the swell and wind sea climate by the Jason-1 mission: a revisit. J. Atmos. Ocean. Technol. 30 (8), 1833–1841.
Jiang, H., Yang, Z., 2022. A revisit of global wind-sea and swell climate and variability using multiplatform altimeters. Rem. Sens. Environ. 271, 112922.
Jiang, H., Babanin, A.V., Chen, G., 2016. Event-based validation of swell arrival time. J. Phys. Oceanogr. 46 (12), 3563–3569.
Kahma, K.K., 1981. A study of the growth of the wave spectrum with fetch. J. Phys. Oceanogr. 11, 1503–1515.
Komen, G.J., Hasselmann, S., Hasselmann, K., 1984. On the existence of a fully developed wind-sea spectrum. J. Phys. Oceanogr. 14, 1271–1285.
Lin, Y.P., Huang, C.J., Chen, S.H., Doong, D.J., Kao, C.C., 2017. Development of a GNSS buoy for monitoring water surface elevations in estuaries and coastal areas. Sensors 17 (1), 172.
Longuet-Higgins, M.S., 1957. On the transformation of a continuous spectrum by refraction. Proc. Camb. Phil. Soc. 53, 226–229.
Mahrt, L., 2011. Surface wind direction variability. J. Appl. Meteorol. Climatol. 50, 144–152.
Meng, W., Li, S., Wang, X., Jiang, H., 2023. Wind-sea and swell separation of 1D wave spectrum by deep learning. Ocean Eng. 270, 113672.
Mitsuyasu, H., Rikiishi, K., 1978. The growth of duration-limited wind waves. J. Fluid Mech. 85, 705–730. Corrigendum, 87, 796–797.
Munk, W.H., Arthur, R.S., 1952. Wave intensity along a refracted ray. In: Proceeding of Symposium on Gavity Waves, 521. U.S. Natl. Bur. Stand. Circ., pp. 95–108
Muraleedharan, G., Kurup, P.G., Sinha, M., Rao, A.D., Latha, G., Dube, S.K., 2010. A theoretical spectrum for multi-peaked energy sea states. International Journal of Oceanography and Marine Science 1 (1), 11–21.
Pierson, W.J., Moskowitz, L., 1964. A proposed spectral form for fully developed wind seas based on the similarity theory of S. A. Kitaigorodskii. J. Geophys. Res. 114, 5181–5190.
Polidoro, Andrea, Pullen, Tim, Eade, Jack, Mason, Travis, Blanco, Belen, Wyncoll, David, 2018. Gravel beach profile response allowing for bimodal sea states. Proceedings of the Institution of Civil Engineers - Maritime Engineering 171 (4), 145–166.
Portilla, J., Ocampo-Torres, F.J., Monbaliu, J., 2009. Spectral partitioning and identification of wind sea and swell. J. Atmos. Ocean. Technol. 26, 107–122.

Qian, C., Jiang, H., Wang, X., Chen, G., 2020. Climatology of wind-seas and swells in the China seas from wave hindcast. J. Ocean Univ. China 19, 90–100.
Quanduo, G., Komen, G., 1993. Directional response of ocean waves to changing wind direction. J. Phys. Oceanogr. 23 (7), 1561–1566.
Romero, L., Melville, W.K., 2010. Airborne observations of fetch-limited waves in the gulf of tehuantepec. J. Phys. Oceanogr. 40, 441–465.
Sverdrup, H.U., Munk, W.H., 1947. Wind, Sea and Swell: Theory of Relations for Forecasting. Navy Hydrogr. Off., Washington, D.C.: U.S. Publ. No. 601.
Tao, A., Yan, J., Pei, Y., Zheng, J., Mori, N., 2017. Swells of the East China Sea. J. Ocean Univ. China 16, 674–682.
Toba, Y., 1978. Stochastic form of the growth of wind waves in a single-parameter representation with physical interpretation. J. Phys. Oceanogr. 8, 494–507, 1978.
Toffoli, A., Babanin, A.V., Onorato, M., Waseda, T., 2010. Maximum steepness of Oceanic waves : field and laboratory experiments. Geophys. Res. Lett. 37.
Tolman, H.L., 2009. User manual and system documentation of WAVEWATCH III TM version 3.14. MMAB contribution 276 (220). Technical note.
Tracy, B., Devaliere, E.-M., Nicolini, T., Tolman, H.L., Hanson, J.L., 2007. Wind sea and swell delineation for numerical wave modeling. In: Proc. 10th Int. Workshop on Wave Hindcasting and Forecasting and Coastal Hazard Symp. U.S. Army Engineer Research & Development Center, Oahu, HI, p. P12.
Tulin, M.P., Waseda, T., 1999. Laboratory observations of wave group evolution, including breaking effects. J. Fluid Mech. 378, 197–232.
Van der Molen, W., Ligteringen, H.J., Van der Lem, C., et al., 2003. Behavior of a moored LNG ship in swell waves. In: Journal of Waterway, Port, Coastal, and Ocean Engineering, 129. ASCE, pp. 15–21.
Van Vledder, G.P., Holthuijsen, L.H., 1993. The directional response of ocean waves to turning winds. J. Phys. Oceanogr. 23 (2), 177–192.
Vartdal, L., Barstow, S.F., 1987. A Separation Algorithm for Wind Sea and Swell for Applications to Directional Metocean Data Buoy. Oceanographic Center, SINTEF Group Tech. Rep. ANODA-30, Trondheim, Norway, p. 104.
Voorrips, A.C., Makin, V.K., Hasselmann, S., 1997. Assimilation of wave spectra from pitch-and-roll buoys in a north sea wave model. J. Geophys. Res. 102, 5829–5849.
Wandres, M., Aucan, J., Espejo, A., Jackson, N., De Ramon N'Yeurt, A., Damlamian, H., 2020. Distant-source swells cause coastal inundation on Fiji's coral Coast. Front. Mar. Sci. 7, 546.
Wang, D.W., Gilhousen, D., 1998. Separation of seas and swells from NDBC buoy wave data. Fifth Int. Workshop on Wave Hindcasting and Forecasting. ASCE, Melbourne, FL, pp. 155–162.
Wang, D.W., Hwang, P.A., 2001. An operational method for separating wind sea and swell from ocean wave spectra. J. Atmos. Ocean. Technol. 18, 2052–2062.
Waseda, T., Tulin, M.P., 1999. Experimental study of the stability of deep-water wave trains including wind effects. J. Fluid Mech. 401, 55–84.
Waseda, T., Toba, Y., Tulin, M.P., 2001. Adjustment of wind waves to sudden changes of wind speed. J. Oceanogr. 57, 519–533.
Young, I.R., 1999. Wind Generated Ocean Waves, 288. Elsevier, New York.
Young, I.R., 2006. Directional spectra of hurricane wind waves. J. Geophys. Res. 111, C08020.
Young, I.R., Vinoth, J., 2013. An extended fetch model for the spatial distribution of tropical cyclone wind-waves as observed by altimeter. Ocean Eng. 70, 14–24.
Yuk, J.H., Kim, K.O., Jung, K.T., Choi, B.H., 2016. Swell prediction for the Korean Coast. J. Coast Res. 32 (1), 131–141.
Zhang, Z., Li, X.M., 2017. Global ship accidents and ocean swell-related sea states. Nat. Hazards Earth Syst. Sci. 17 (11), 2041–2051.
Zheng, Z., Dong, G., Dong, H., Ma, X., Tang, M., 2024. Research on the methods for separating wind sea and swell from directional wave spectra in finite-depth waters. Ocean Dyn. 74 (2), 113–131.